A general mixed mode fracture mechanics test specimen: The DCB-specimen loaded with uneven bending moments

Sørensen, Bent F.; Jørgensen, K.; Jacobsen, T.K.; Østergaard, R.C.

Publication date:
2004

Document Version
Publisher's PDF, also known as Version of record

Risø-R-1394(EN)

A general mixed mode fracture mechanics test specimen: The DCB-specimen loaded with uneven bending moments

Bent F. Sørensen, Kenneth Jørgensen, Torben K. Jacobsen, and Rasmus C. Østergaard

Materials Research Department,
Risø National Laboratory, 4000 Roskilde, Denmark

LM Glasfiber, Rolles Møllevej 1,
DK-6640 Lunderskov, Denmark

Risø National Laboratory, Roskilde
March 2004

Abstract

A mixed mode specimen is proposed for fracture mechanics characterisation of adhesive joints, laminates and multilayers. The specimen is a double cantilever beam specimen loaded with uneven bending moments at the two free beams. By varying the ratio between the two applied moments, the full mode mixity range from pure mode I to pure mode II can be generated for the same specimen geometry. The specimen allows stable crack growth. In case of large scale crack bridging, mixed mode cohesive laws can be obtained by a J integral based approach. As a preliminary example, fracture of adhesive joints between two glass-fibre laminates was studied. The mixed mode fracture resistance increased with increasing crack length due to fibre cross over bridging, eventually reaching a steady-state level (R-curve behaviour). The steady-state fracture toughness level increased with increasing tangential crack opening displacement. Cohesive stresses were determined by a J integral approach. The deducted shear stress was found to be relative high (≈ 20 MPa) in comparison with the normal stress (≈ 1 MPa).

ISBN 87-550-3186-2
ISBN 87-550-3187-0(Internet)
ISSN 0106-2840

Print. Pitney Bowes Management Services A/S 2004

Contents

Preface

This report contains a description of some of the work that was carried out in a project called "Improved design for large wind turbine blades, based on studies of scale-effects (Phase 1)", partially supported by the Danish Energy Authority under the Ministry of Economics and Business Affairs through a EFP2001-fund (journal no. 1363/01-01-0007). The project ran 1½ year from 2001 to 2002. The participants in the project were: The Materials Research Department, Risø National Laboratory (project leader), The Wind Energy Department, Risø National Laboratory, The Department of Mechanical Engineering (Solid Mechanics), The Technical University of Denmark, Department of Mechanical Engineering, Aalborg University, LM Glasfiber A/S and Vestas Wind Systems A/S. It was found to be impossible to acquire students at Aalborg University. As a result, no work was performed there. Instead, more work was carried out at Risø National Laboratory.

This report only contains the description of the development of a new fracture mechanics test method and some initial results obtained from fracture mechanics test specimens. The specimens were manufactured by LM Glasfiber A/S/ and tested the specially developed fixture at the Materials Research Department, Risø National Laboratory. The major results of the entire project can be found in the summary-report, which also contains a list of the publications that came out of the project:

Risø-R-1390(EN)
"Fundamentals for improved design of large wind turbine blade of fibre composites based on studies of scale effects (Phase 1) - Summary Report" , Bent F. Sørensen, Erik Jørgensen, Christian P. Debel, Find M. Jensen and Henrik M. Jensen, ISBN 87-550-3176-5; ISBN 87-550-3177-3(Internet) ISSN 0106-2840

1 Introduction

Many modern components, from microchips to ships and large wind turbine blades are made of materials arranged in layers. Mixed mode cracking is commonly observed in such structures, since they often have weak planes. Examples of failure modes are delamination of laminates and interface cracks in sandwich structures, adhesive joints and multilayered structures. Earlier studies have shown that the interfacial fracture energy, expressed in terms of the critical energy release rate, $\mathcal{G}_c$, can depend on the mode mixity. Usually, the critical energy release rate increases when the amount of tangential displacement ("mode II") near the crack tip becomes larger than the crack opening displacement ("mode I") (Cao and Evans, 1989; Wang and Suo, 1990; Thouless, 1990; Lichti and Chai, 1992). The increase in macroscopic fracture energy with increasing amount of crack tip sliding has been attributed to various mechanics, such as crack face contact by asperities near the crack tip (Evans & Hutchinson, 1989), to differences in the crack tip plasticity (Tvergaard and Hutchinson, 1993) and to electrostatic effects between the crack faces (Liang and Liechti, 1995).

Cracking of fibre composites is often accompanied by fibre bridging. Fibres or fibre ligaments remain attached to both crack faces and thus create multiple connections between the crack faces behind the crack tip. The bridging fibres restrain the crack opening and raise the fracture resistance (R-curve behaviour), see e.g. Suo et al. (1992). The fracture toughness enhancement due to fibre bridging can be large in comparison with the crack tip fracture energy (Albertsen et al., 1995; Sørensen and Jacobsen, 1998; Feih et al., 2003).

Basically, crack bridging is a large-scale failure process zone and cannot be characterised in terms of linear elastic fracture mechanics (LEFM). Instead, the failure process zone can be modelled by non-linear fracture mechanics, e.g. by a cohesive zone model (Foote et al., 1986; Cox and Marshall, 1991; Suo, Bao Fan, 1992; Östlund, 1995). Crack bridging is then represented by surface tractions along the crack face. The relationship between the local traction and the local opening is usually taken to be a material property called the cohesive law (Bao and Suo, 1992). A useful tool in the analysis of bridged cracks is the path independent J integral (Rice, 1968), which can be applied to large scale bridging problems (Suo et al., 1992).

Many LEFM mixed mode and mode II test configurations, e.g. used to characterise laminates, rely on loading specimens by transverse forces (Williams, 1989; Reeder and Crew, 1992; Shivakumar et al., 1998; Hashemi et al., 1990). For those specimens it is not possible to determine the J integral in closed analytical form when large scale bridging occurs (Bao and Suo, 1992; Sørensen and Jacobsen, 2000). Also, for mixed mode specimens, crack growth may be unstable (Ozdil and Carlsson, 2000). Furthermore, such mode II specimens are susceptible to friction between the beams at the points where the transverse forces are applied (Williams, 1989; Hashemi et al., 1990). By the use of these test methods, it is therefore difficult to investigate whether toughening mechanisms occurs and to quantify their toughening effects.

Until now, approaches to extract the mixed mode cohesive laws require significant computational efforts e.g. by incremental finite element models of test

specimens to fit global specimen response e.g. the load-displacement curve (Yang et al., 1999; Kafkalidis and Thouless, 2002) or a near-tip displacement field (Mohammed and Liechti, 2000; Liechti and Wu, 2001). Typically, a number of finite element analysis with different cohesive zone parameters are performed, before the correct cohesive law parameters are identified. Obviously, it is of interest to develop simpler approaches for the measurements of mixed mode cohesive laws.

It is desirable to characterise mixed mode cracking parameters by specimens that: (i) allows stable crack growth, (ii) allows the full range of mode mixity, and (iii) can be used for characterising specimens that experience large scale bridging, i.e. characterising cohesive laws. Furthermore, it is preferable to use the same specimen geometry for all mode mixities so that possible error sources associated with processing variation can be eliminated.

The purpose of the present paper is to develop a fairly general fracture mechanics method for characterising mixed mode crack growth. The proposed specimen full fills the requirements described above. Mixed mode cohesive laws can be determined by a J integral approach. In previous studies, cohesive laws have been determined for symmetric crack opening (mode I) (Sørensen and Jacobsen, 1998; Feih et al., 2003). Therefore, in this study our aim is to investigate the effect of fibre cross over bridging under mixed mode, particularly under dominating mode II.

The paper is organised as follows: First, the basic mechanics of the proposed specimen is presented. Next, we describe the practical implementation of the concept and describe the test arrangement that we have developed. Then, we illustrate the capability of the approach by some measurement of cohesive laws, representing fibre cross over bridging in adhesive joints. Finally, advantages and drawbacks of the methods are discussed and major conclusions are drawn.

2 Basic mechanics

The proposed specimen is shown in Fig. 1. It consists of a double cantilever beams (DCB) specimen loaded with uneven bending moments (DCB-UBM) at the two beams. In the following we analyse the DCB-UBM specimen under two different conditions, viz. under the assumption of a small scale failure process zone and under large scale bridging (LSB). In both cases, isotropic linear elastic properties are assumed outside the failure process zone. In plane stress, the only stress component that enters the analysis is the normal stress in the direction parallel to the specimen. Only the Young's modulus in the direction parallel to the specimen enters the equation. Thus, extensions to ortotropic materials are straightforward (Suo, 1990). Small strains and small displacements are assumed.

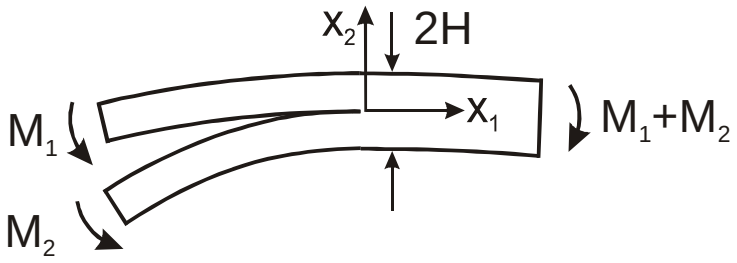

Figure 1. A homogenous mixed mode facture mechanics test specimen: The double cantilever beam specimen loaded with uneven bending moments (DCB-UBM). [Mixed_mode_specimens_1g.cdr]

2.1 Calculation of J integral from applied moments

When the beams outside the failure process zone are longer than a few times the beam height, the energy release of the specimen is independent of crack length. The energy release rate can be calculated by evaluating the path independent J integral (Rice, 1968) along a path along the external boundaries of the specimen (Fig. 2a), Γ_{ext}. The only non-zero contributions come from the beam-ends, which are subjected to pure bending. The result for the homogenous DCB-UBM specimen shown in Fig. 1 is (plane strain)

$$J_{ext} = \left(1-\nu^2\right) \frac{21\left(M_1^2 + M_2^2\right) - 6M_1M_2}{4B^2H^3E} \ , \qquad (1)$$

where M_1 and M_2 denote the applied bending moments (positive signs are shown in the figure), E and ν denotes the Young's modulus and the Poisson's ratio, B is the specimen width and H is the beam height. For plane stress, the terms $1-\nu^2$ should be replaced by unity. Note that the energy release rate is independent of crack length; the DCM-UBM is a steady-state specimen.

Sandwich specimens, e.g. specimens where two skin layers are joined by a thin core layer that is much thinner than other relevant specimen dimensions, are often used for characterising interfacial crack growth in bimaterial specimens. This type of specimen is attractive since, if cracking occurs along the interface so that the core layer remains attached to one of the skin layers, the residual stresses do not contribute to the energy release rate (Wang and Suo, 1990). Then, (1) remains valid. However, if the core thickness, h, is not much smaller than the thickness of the skins, H, the core thickness must be taken into account, as in the following. A DCB-UBM sandwich specimen is shown in Fig. 3. Residual stresses are ignored in the following; an analysis of this is given elsewhere (Østergaard and Sørensen, 2003). The J integral evaluated along the external boundaries of the sandwich specimen gives (plane strain)

$$J_{\text{ext}} = \frac{1-\nu_2^2}{B^2H^3E_2}\left\{\frac{M_1^2}{2\eta^3 I_0} + 6M_2^2 - \frac{\left(M_1+M_2\right)^2}{2\eta^3 I_1}\right\}, \qquad (2)$$

where H and E_2 denote the thickness and the Young's' modulus, respectively, of the skin layers (material #2). For plane stress, the terms $1-\nu_2^2$ should be replaced by unity. The non-dimensional parameters η, I_0 and I_1 depend on the

stiffness properties and layer thickness as described in Appendix A. Equations (1) and (2) are valid for both small-scale failure process zone and for large scale bridging problems.

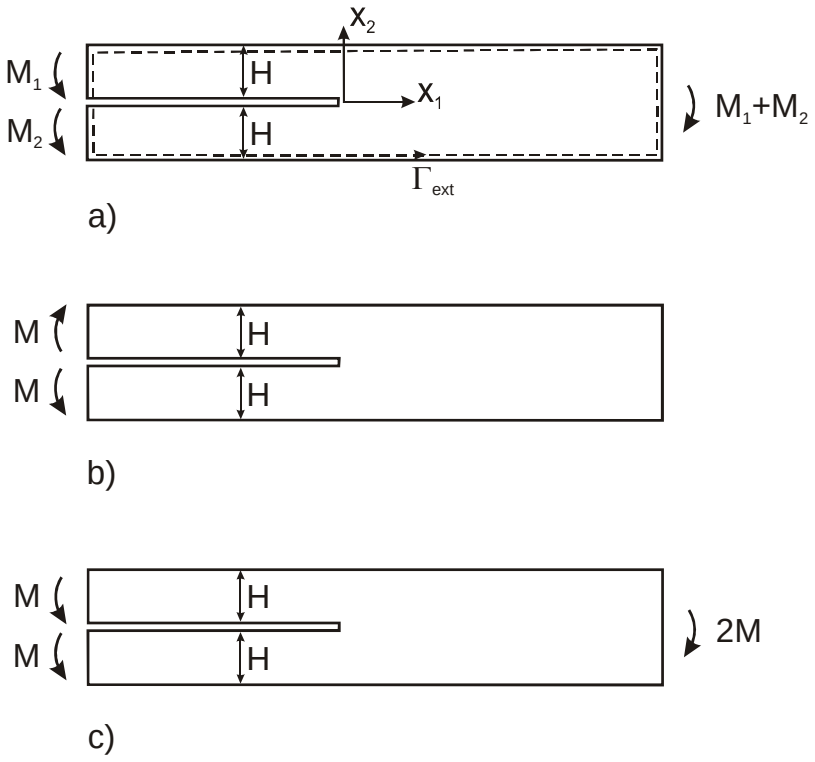

Figure 2. The homogenous mixed mode specimen (a), can be obtained by superposition of a pure mode I specimen (b) and a pure mode II specimen (c). [Mixed_mode_specimens_1g.cdr]

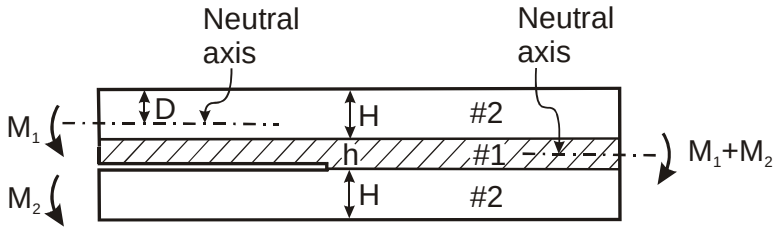

Figure 3. Geometry and loading of a DCB-UBM sandwich specimen. [Mixed_mode_sandwich_1a.cdr]

2.2 Small scale failure process zone parameters: Energy release rate and mode mixity

LEFM is applicable when the failure process zone is much smaller than the smallest specimen dimension (for DCB-specimens, the beam height, *H*). Then, for crack propagation along a weak plane, an appropriate failure criterion is of the form (Jensen et al., 1990; Hutchinson and Suo, 1992)

$$\mathcal{G}(\psi) = \mathcal{G}_c(\psi) \qquad (3)$$

where $\mathcal{G}$ is the energy release rate, $\mathcal{G}_c$ is the critical energy release rate, ψ is the mode mixity, defined as the phase angle of the stress intensity factors (Hutchinson and Suo, 1992),

$$\psi = \tan^{-1}\left(\frac{K_{II}}{K_I}\right) \tag{4}$$

with K_{II} and K_I being the mode II and mode I stress intensity factors, respectively. Recall, that for LEFM, $J_{ext} = \mathcal{G}$ (Rice, 1968).

The *homogenous* specimen (Fig. 2a) can be constructed by a superposition of a pure mode I specimen (Fig. 2b) and a pure mode II specimen (Fig. 2c), both analysed by Hutchinson and Suo (1992). Then, ψ can be obtained as

$$\psi = \tan^{-1}\left(\frac{\sqrt{3}}{2}\frac{M_1 + M_2}{M_2 - M_1}\right) \tag{5}$$

Plots of J and ψ as a function of the ratio between the moments are shown in Fig. 4. J and ψ are both well-behaving in the sense that rapid variations, with respect to M_1/M_2, do not occur. The practical implication is that it is not necessary to control M_1/M_2 with a high degree of accuracy. Small changes in M_1/M_2 during an experiment do not change neither J nor ψ significantly.

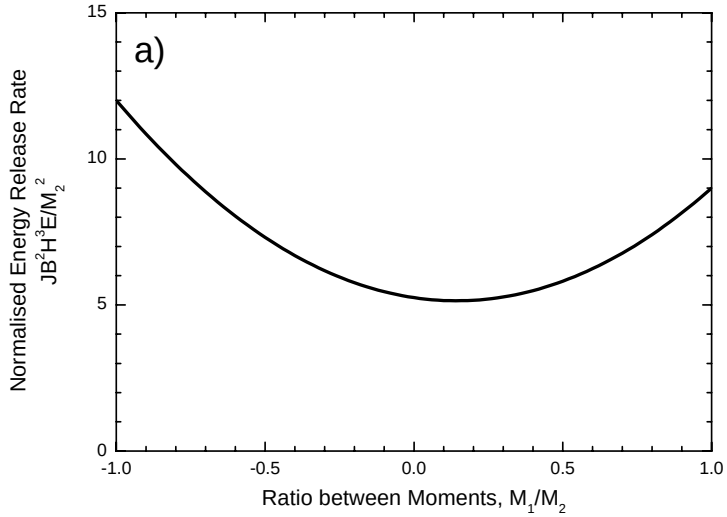

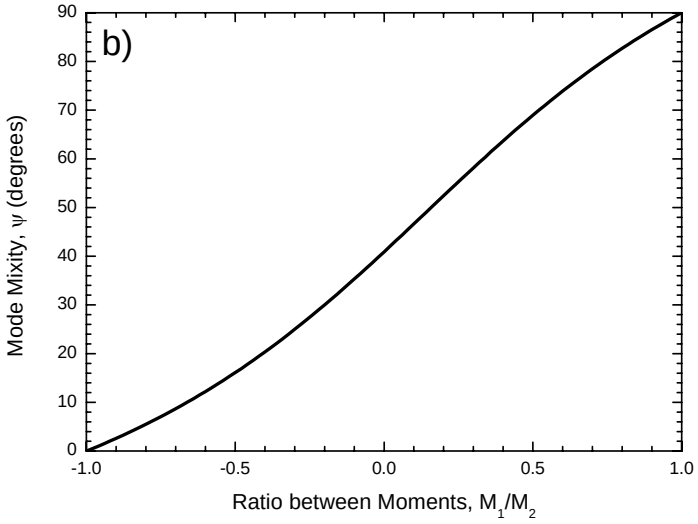

Figure 4. Plots of a) the normalised J integral value of the DCB-UBM specimen as a function of the ratio between the applied moments, b) the resulting mode mixity a function of the ratio between the applied moments. [Moments_mixity_1d.opj]

For *sandwich* specimens possessing a small-scale failure process zone, an appropriate fracture criterion for interfacial crack growth can be formulated similar to equation (3), but using a slightly different definition for the mode mixity. The mode mixity of an interface crack is usually defined as (Hutchinson and Suo, 1992)

$$\widehat{\psi} = tan^{-1}\left(\frac{Im\left(KH^{i\varepsilon}\right)}{Re\left(KH^{i\varepsilon}\right)} \right) , \qquad (6)$$

where now $K = K_1 + iK_2$ is the complex stress intensity factor characterising the stress state at a bimaterial crack tip (Rice, 1988), ε is a bimaterial constant, $i = \sqrt{-1}$, while Re($KH^{i\varepsilon}$) and Im($KH^{i\varepsilon}$) indicate real- and imaginary parts of $KH^{i\varepsilon}$, respectively. The non-dimensional parameter ε depends on the stiffness mismatch of the two materials, see e.g. Rice (1988) and Hutchinson and Suo (1992) for details. For identical materials, ε = 0. Then equation (6) reduces to (4), $\widehat{\psi} = \psi$.

For the sandwich specimen, $\widehat{\psi}$ depends on M_1/M_2, h/H and two non-dimensional stiffness parameters defined elsewhere (Dundurs, 1969). When the core thickness is *very small*, the mode mixity of the interface crack, $\widehat{\psi}$, can be determined by the remote mode mixity ψ of the homogeneous specimen (equation (5)) except for a stiffness mismatch-dependent shift angle, that has been determined by Suo and Hutchinson (1989). The mode mixity of the interface crack in DCB-UBM sandwich specimens having a *finite core thickness* can be obtained from the analysis of Østergaard and Sørensen (2003).

2.3 Specimens experiencing large scale bridging: Determination of cohesive laws

Large scale bridging (LSB) is defined as the situation where a failure process zone in a specimen is large only in the length direction of the crack, i.e., its dimension in the direction perpendicular to the crack plane is very small. Under LSB, LEFM cannot be applied. Consequently, fracture should not be characterised in terms of $\mathcal{G}_c(\psi)$. Rather, the *failure process zone* can be modelled as a *cohesive zone* in which the crack faces are connected by tractions, described in terms of a so-called cohesive law.

It is common to assume, that within the cohesive zone the local cohesive tractions depend only on the local normal and tangential crack opening displacements, denoted δ_n and δ_t respectively,

$$\sigma_{22} = \sigma_{22}(\delta_n, \delta_t) \quad \sigma_{12} = \sigma_{12}(\delta_n, \delta_t) , \qquad (7)$$

where σ_{22} is the normal stress and σ_{12} is the shear stress transmitted across the crack faces within the cohesive zone. The relationships (7) are the *mixed mode cohesive laws*. The cohesive laws are assumed to be material properties and identical at each points along the cohesive zone. However, since δ_n and δ_t vary as function of position along the cohesive zone, so do σ_{22} and σ_{12}. The path independent J integral can be applied to LSB problems (Suo et al. 1992). Evaluation the J integral along an integration path, Γ_{loc}, that runs locally along the cohesive zone, enclosing the crack tip (see Fig. 5) gives

$$J_{loc} = \int_0^{\delta_n^*} \sigma_{22}(\delta_n, \delta_t) d\delta_n + \int_0^{\delta_t^*} \sigma_{12}(\delta_n, \delta_t) d\delta_t + J_{\text{tip}} , \quad (8)$$

where δ_n^* and δ_t^* are the end-opening and end-sliding of the cohesive zone and J_{tip} is the J integral evaluated around the crack tip. Physically, eq. (8) can be interpreted as follows: The J integral comprises two contributions from the cohesive zone (the energy uptake by normal and shear stresses, the two integrals) and a contribution from the crack tip. As suggested by (8), the toughening from the cohesive zone depends on the ratio of the end-sliding and end-opening. The maximum toughening (achieved when the cohesive zone is fully developed and σ_{22} and σ_{12} both vanish at the end-opening) is thus also expected to depend on the ratio between the end-sliding and end-opening of the cohesive zone. In cohesive zone models, the cohesive laws can be implemented as non-linear springs. Crack propagation occurs when J_{tip} reaches the fracture energy of the crack tip, J_0, which is assumed to be a material property independent of crack tip mode mixity.

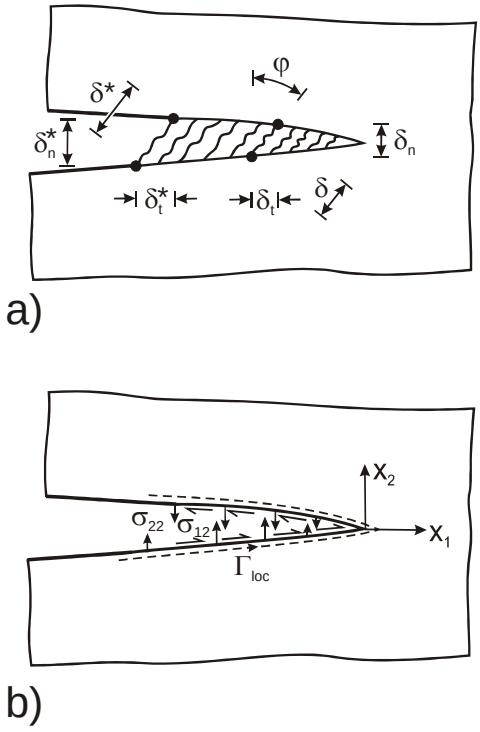

Figure 5. Mixed mode cohesive zone parameters: a) Definition of crack opening parameters, and b) integration paths for the J integral: locally around the crack faces and crack tip, Γ_{loc}. [Mixed_mode_crack_tip_model_1b.cdr]

When the length of the un-bridged beams is larger than a few times the beam height, J_{ext} is still given by (1) or (2). This is true even though a large-scale bridging zone is present in the specimen; for the DCB-UBM specimen, unlike most other mixed mode fracture mechanics test specimens, J_{ext} can be determined from the applied moments and specimen geometry without any knowledge about the details of the cohesive law (obviously, due to path independency, $J_{ext} = J_{loc}$, so that J_{ext} depends on the cohesive stresses. However, during an experiment, J_{ext} can be determined from the applied moments and the specimen geometry). This prominent feature makes these specimens (Figs. 1 and 2) suitable for determination of the cohesive laws.

Assume that the cohesive laws can be derived from a displacement potential, $\Phi(\delta_n, \delta_t)$, as

$$\sigma_{22}(\delta_n,\delta_t) = \frac{\partial\Phi(\delta_n,\delta_t)}{\partial\delta_n} \quad \sigma_{12}(\delta_n,\delta_t) = \frac{\partial\Phi(\delta_n,\delta_t)}{\partial\delta_t}. \quad (9)$$

Inserting (9) into (8) and performing the integration gives

$$J_{loc} = \Phi(\delta_n^*,\delta_t^*) + J_{tip}. \quad (10)$$

During cracking, J_{tip} is assumed to be constant, being equal to the fracture energy of the crack tip, J_0. This assumption is justified by the fact that for composites experiencing fibre bridging, the crack tip fracture energy is usually significantly smaller than the energy uptake by the bridging zone. Also, even though the crack tip fractue energy may vary as a function of the crack tip mode mixity

(Liechti and Chai, 1992), the mode mixity is unlikely to vary much during an experiment in which the loads are applied proportional to each other. The energy uptake in the cohesive zone, $\Phi\left(\delta_n^*, \delta_t^*\right)$, increases as δ_n^* and δ_t^* increase. Therefore, the fracture resistance, J_R - the value of the J integral during crack growth -, increases with increasing crack length (R-curve behaviour),

$$J_R = \Phi\left(\delta_n^*, \delta_t^*\right) + J_0 . \qquad (11)$$

Usually, the fracture resistance reaches a steady-state value, J_{ss}. The failure process zone is then fully developed. With further cracking, the cohesive stresses vanish at the end-opening, and the failure process zone then translates along the specimen in a self-similar fashion under steady–state conditions.

As J_{tip} is assumed to be constant (equal to J_0) during cracking, it follows that the cohesive stresses at the end of the cohesive zone (where, per definition, $\delta_n = \delta_n^*$ and $\delta_t = \delta_t^*$) can be determined from

$$\sigma_{22}\left(\delta_n^*, \delta_t^*\right) = \frac{\partial J_R}{\partial \delta_n^*} \qquad \sigma_{12}\left(\delta_n^*, \delta_t^*\right) = \frac{\partial J_R}{\partial \delta_t^*} \ . \qquad (12)$$

Thus, by measuring J_R – calculated according to (1) or (2) -, δ_n^* and δ_t^* during cracking, the cohesive law can be determined by (12). This approach will be utilised later in the paper.

Under LSB, the mode mixity, (5)-(6), losses its significance as a parameter characterising the stress field around the failure process zone. Instead, the parameters δ_n^* and δ_t^* are the relevant parameters, as seen e.g. from (8). At a given position within the cohesive zone, the normal- and tangential crack opening displacements can be expressed through the magnitude of the crack opening displacement and the phase angle of the opening, defined as

$$\delta = \sqrt{\delta_n^2 + \delta_t^2} \ \text{and} \qquad \varphi = \tan^{-1}(\delta_t / \delta_n) \ , \qquad (13)$$

where $\varphi = 0°$ is pure normal opening and $\varphi = 90°$ corresponds to pure tangential crack opening displacements. In particular, the magnitude and phase angle of the end-opening just when J_{ss} is attained (i.e., when the cohesive stresses vanish) are defined as

$$\delta_0 = \sqrt{\delta_n^{0^2} + \delta_n^{0^2}} \ \text{and} \ \varphi_0 = \tan^{-1}\left(\delta_t^0 / \delta_n^0\right) \qquad (14)$$

where δ_n^0 and δ_t^0 indicate the values of the end-opening and end-sliding where the cohesive stresses vanish.

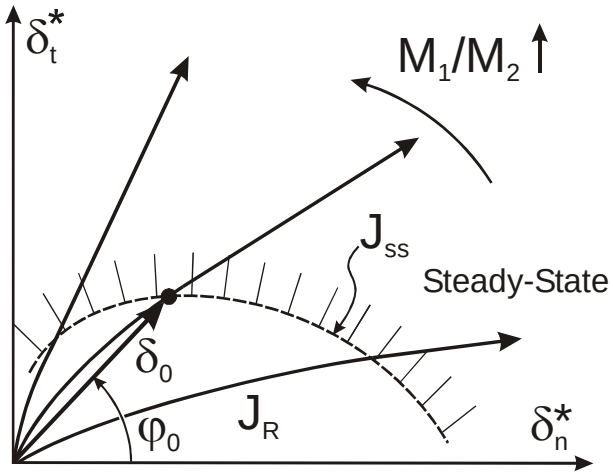

Figure 6. Schematic diagram that shows different paths for end-opening and end-sliding during monotonically increasing loading. A curve, $\delta_0(\varphi_0)$, demarks the domain with rising fracture resistance and the steady-state fracture resistance. [End_Opening_Paths_1a.cdr]

Fig. 6 illustrates expected relationships between end-opening and end-sliding during monotonic loading experiments of DCB-UBM specimens. Different lines represent experiments conducted under different M_1/M_2-ratios. For each experiment M_1/M_2 remains fixed. A dominating opening mode ("mode I") ($\delta_n^* > 0$ and $\delta_t^* \approx 0$) is anticipated for $M_1 > 0$ and $M_2 \approx -M_1$, while a domination "mode II" ($\delta_t^* > 0$ and $\delta_n^* \approx 0$) is expected for $M_1 > 0$ and $M_2 \approx M_1$. Irrespective of the M_1/M_2-ratio, the fracture resistance increases in accordance with (11) until the steady-state value is reached. The onset of steady-state is marked by the curve $\delta_0(\varphi_0)$. Beyond $\delta_0(\varphi_0)$, a steady-state fracture resistance

$$J_{ss} = \Phi\left(\delta_n^0, \delta_t^0\right) + J_0 \qquad (15)$$

is expected since the failure process zone is fully developed and it is expected that with continuing cracking the cohesive zone merely translate along the specimen in a self-similar fashion so that the size of the cohesive zone and phase angle of the end opening of the active zone, $\varphi_0 = \tan^{-1}\left(\delta_t^0 / \delta_n^0\right)$, remain the same. Such a steady-state behaviour is unique to the DCB-UBM specimen and its family of test specimens (Suo et al., 1992). For other specimens the cohesive zone length and phase angle of the end-opening of the active zone changes during crack growth. Therefore, for these specimens no steady-state is expected.

3 Experimental procedures

3.1 Test fixture

The principle of creating different bending moments in the two free beams of the DCB-UBM specimen is shown schematically in Fig. 7. Forces of identical magnitude, $P/2$, are applied perpendicular to two transverse beams connected to the end of the beams of the DCB specimen. The un-cracked end of the specimen is restricted from rotation but can move freely in the x_1-direction. Different moments are obtained if the length of the two moment arms, ℓ_1 and ℓ_2, of the transverse beams are different. The applied moments are then

$$M_1 = \frac{P\ell_1}{2} \qquad \text{and} \qquad M_2 = \frac{P\ell_2}{2}\,. \qquad (16)$$

It follows from (16) that the mode mixity (equation (5)) can be changed simply by altering one moment arm, say ℓ_1, so that $-1 \le \ell_1/\ell_2 \le 1$ (ℓ_1 being taken positive when the force closest to the specimen acts in the x_2-direction, as shown in Fig. 7).

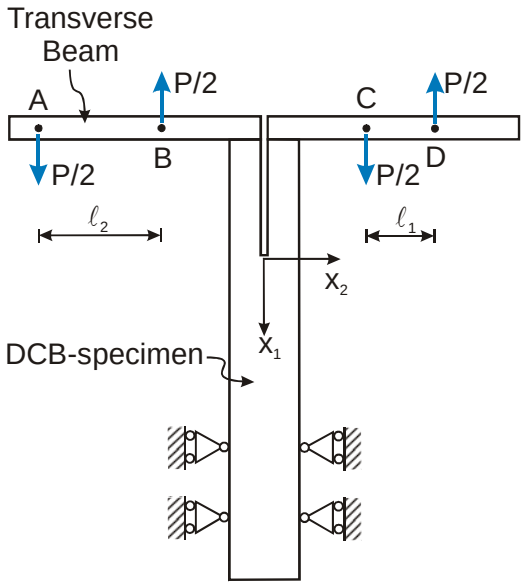

Figure 7. Schematics of the proposed loading method; the mode mixity is controlled entirely by altering the length of one of the transverse beam arms, e.g. ℓ_1. [Mixed_Mode_loading_1c.cdr]

Identical forces are obtained by the use of a wire arrangement. The idea builds upon earlier fixtures for pure mode I testing (Freiman et al., 1973; Sørensen et al., 1996). A 1.5 mm thick steel wire runs from the upper part of a tensile test machine, mounted at a load cell, via rollers to one of the transverse beams, down to rollers at the lower part of the tensile test machine and up again in a similar manner in the other side of the fixture, see Fig. 8. The rollers at the transverse beams are mounted though holes. This allows easy and well defined adjustments of the moment arms.

Figure 8. Photos of the test set-up. Overview over the test fixture. [Opstilling_udsnit.bmp]

The gravitational forces of the transverse beams (made in aluminium) are outbalanced by helical springs. Some additional considerations were made to minimize errors in the applied moments as the specimen deforms, see Appendix B.

3.2 Specimen manufacturing

Two plates (300 mm by 300 mm, thickness approximately 8 mm) were made of a glass fibre composite. The layup of the laminates was [±45, 0_8, ±45] i.e. almost unidirectional. The plates were made by hand-lay up of dry fibre bundles, followed by matrix impregnation by vacuum infusion and post-cured. The material was thus anisotropic with a major Young's modulus of about 34 GPa and a major Poisson's ratio of 0.25. A thin slip foil was placed at the one end of the plates to act as a pre-crack and ease crack initiation. Then, an adhesive was applied to the surface of the one plate. The other plate was then put on the top of the adhesive. Spacers were used to control the thickness of the adhesive layer. The adhesive was then post-cured. The thickness, *h*, of the adhesive layer was approximately 3 mm. Specimens, 30 mm in width, were cut from the sandwich plates. Steel parts were fixed to each beam by 4 steel screws (M5) and an epoxy adhesive (Scotch-Weld DP 460 from 3M, hardened at 40°C for two hours). The specimen geometry is shown in Fig. 9.

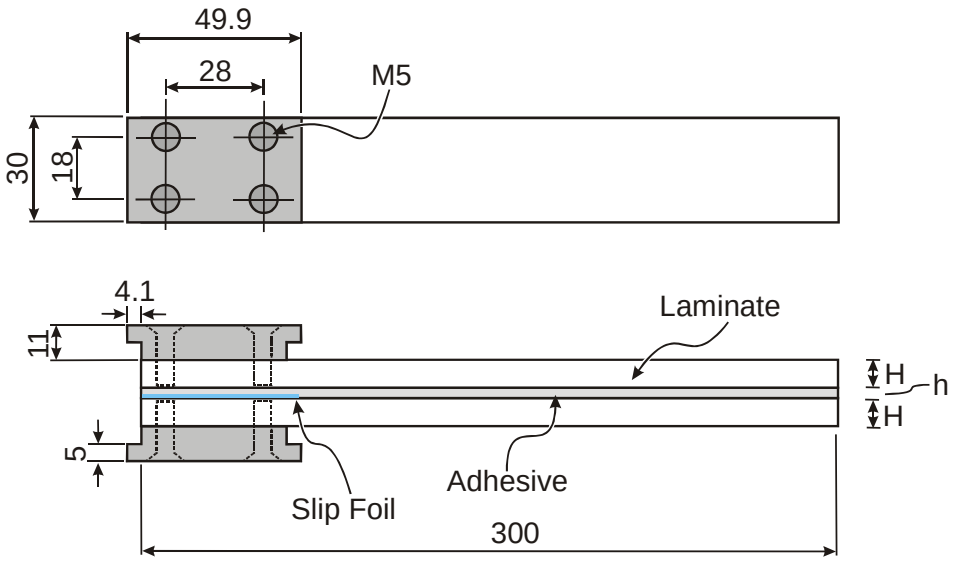

Figure 9. Sketch of the specimen geometry. Steel parts are attached to the laminates by screws and adhesive. Nominal dimensions: H = 8 mm, h = 3 mm and B = 30 mm. [Mixed_mode_specimens_dimensions_1b.cdr]

3.3 Test procedure

The experiments were conducted in two parts, (i) crack initiation and (ii) monotonic loading following re-notching. In the first part the specimen was loaded near-symmetrical loading (M_1/M_2= -0.45) until crack growth initiated. Typically, a significant load drop and a crack extension of about 5-10 mm occurred in connection with crack initiation. The associated crack opening displacement was about 20-40 μm. The rapid crack growth and the associated load drop prevented detailed measurements of the initial part of the cohesive laws. Therefore, the crack tip position was marked up at the side of the specimen before the specimen was unloaded. A cut was made in the middle of the adhesive layer by a band saw until 1-2 mm from the crack tip. The purpose of this re-notching was to create a specimen that had a truly sharp crack tip with very limited fibre bridging.

Following re-notching, steel pins (diameter 1.4 mm) were placed in holes drilled in the laminates at the end-of the inserts. The pins were positioned at the mid-plane of the laminates to minimise their effect on the stress state in the specimen. An extensometer (Instron, type 2620-602) was mounted at the pins, in a way that it could rotate freely and thereby record a crack opening displacement, δ_m, see Fig. 10a. At the other face, an LVDT (H. F. Jensen, type LDI 8/1 MR) was mounted parallel to the adhesive layer in a special holder to record the tangential displacements (denoted δ_t^*) at the end of the cohesive zone, see Fig. 10b. Markers (10 mm apart) were made at a side of the specimen to ease the determination of crack length.

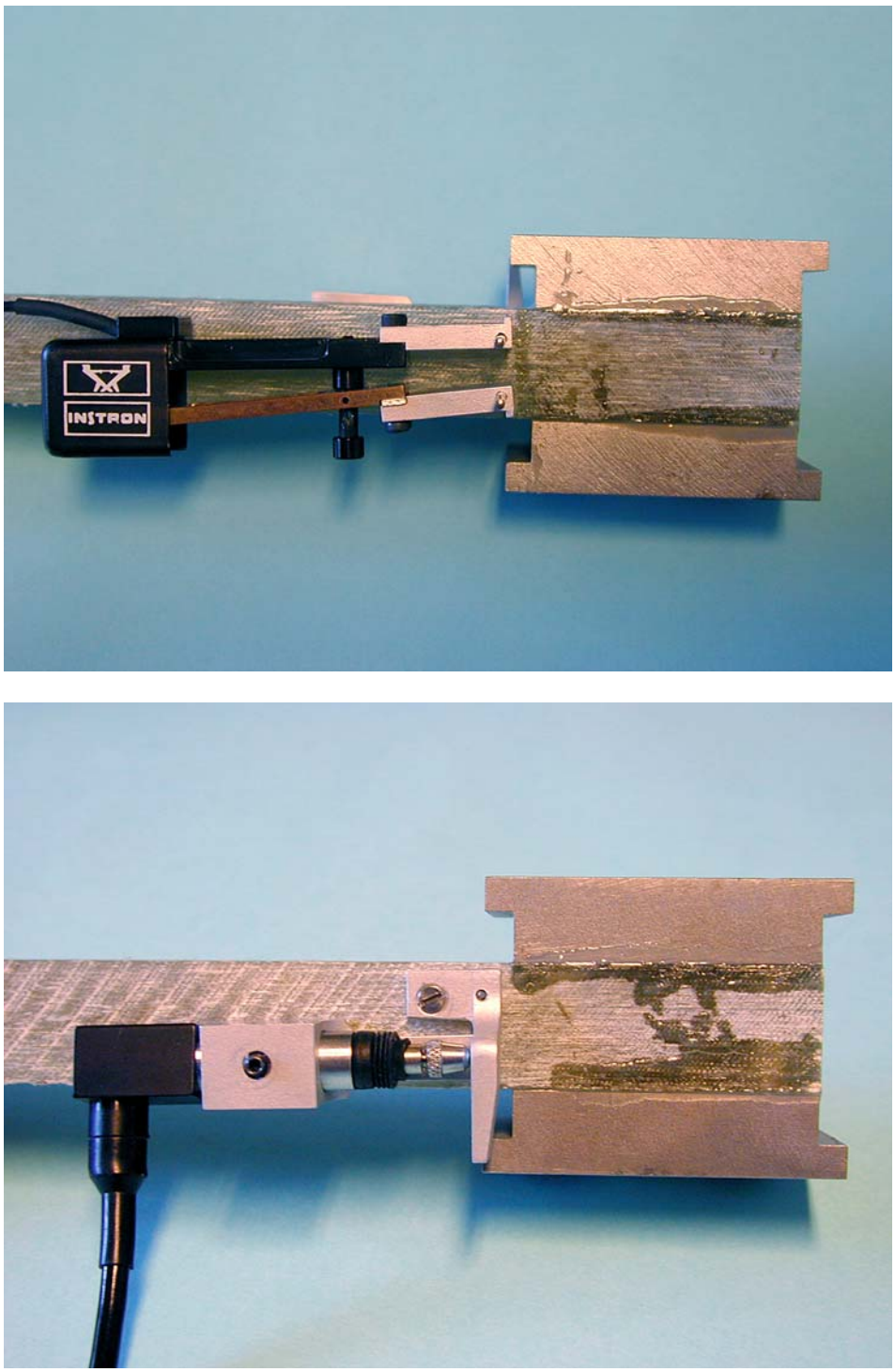

Figure 10. Instruments mounted at the specimen for recording the crack opening displacement, δ_m, by an extensometer (a), and measurement of the end-sliding, δ_t^*, by an LVDT. [Extensometer_01.jpg; LVDT Close Up 01.jpg]

Then, in the second part, the specimen was loaded monotonically at a constant displacement rate (5 mm/min). Data (elapsed time, load, end-opening displacements) were collected (5 Hz) at a computer using a Notebook data acquisition programme. Loading was continued until a stationary load level (indicating steady-state fracture resistance) was achieved.

3.4 Data analysis

The displacement normal to the crack plane, δ_n^*, was calculated by the law of Pythagoras, see Fig. 11b,

$$\delta_n^* = \sqrt{\left(d + \delta_m\right)^2 - \delta_t^{*2}} - d \ , \qquad (17)$$

where d is the initial distance between the points at which the displacements are recorded. In should be noted, that the displacements measurements comprise *both* the stretch of the cohesive zone *and* the elastic deformation of the specimen from $x_2 = -d/2$ to $x_2 = d/2$; however, the elastic deformation is assumed to be so small that it can be neglected (Sørensen and Jacobsen, 2000). In the present experiments the pins are mounted at the neutral axis of the beams, so that $d = H + h$.

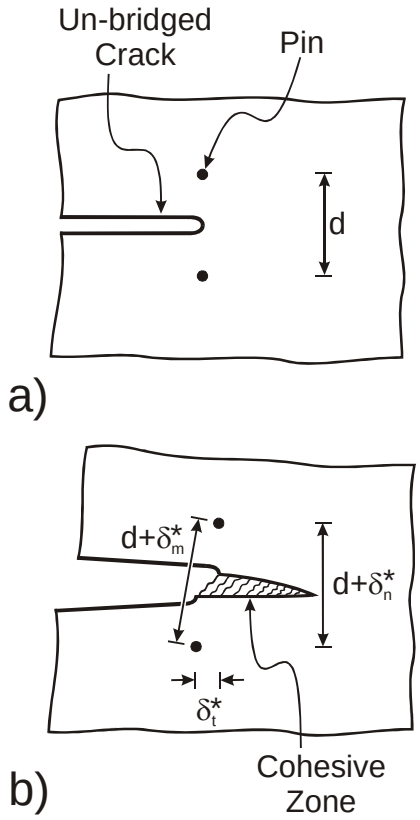

Figure 10b. Schematics illustration showing the geometric relationship between the normal displacement, δ_n^*, and tangential displacement, δ_t^*, and the measured displacement, δ_m: a) before and b) after the development of a cohesive zone. [Mixed_mode_COD_measurements_1c.cdr]

4 Results

4.1 Crack path selection

Fig. 12 shows pictures of some cracking specimens under various mixed mode loadings. Under mixed mode cracking, the crack propagation did not occur within the adhesive layer (traditionally denoted "cohesive failure" in the adhesive literature (Kinloch, 1987; Matthews, 1987), but along the adhesive/laminate interface towards the beam that was subjected to the highest moment. This cracking mode is called “adhesive failure”. The crack path selection is consistent with the well-known observation that crack propagating in a homogenous material usually seeks to grow in a pure mode I path, i.e., a direction where the local crack tip stress fields is pure mode I (ψ = 0 degrees) (Thouless and Evans, 1990). After some, say, 20 mm crack extension, a new crack formed at the next interface within the laminate, between the 0- and 45-degree plies. This cracking mode is delamination. Subsequently, both the delamination crack and the interface crack grew; usually the delamination crack propagated at the highest rate. Fibre cross over bridging was observed for both cracking planes. The measured fracture resistance of the interface crack and the delamination could differ.

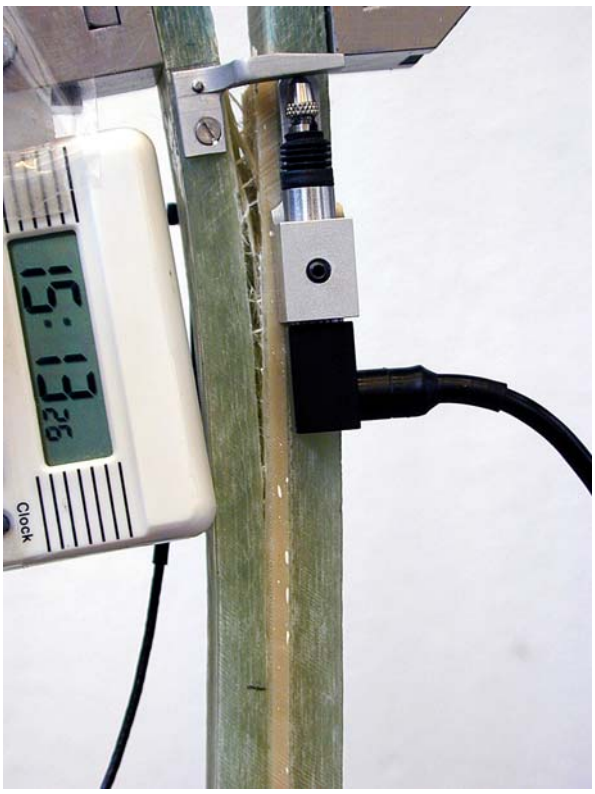

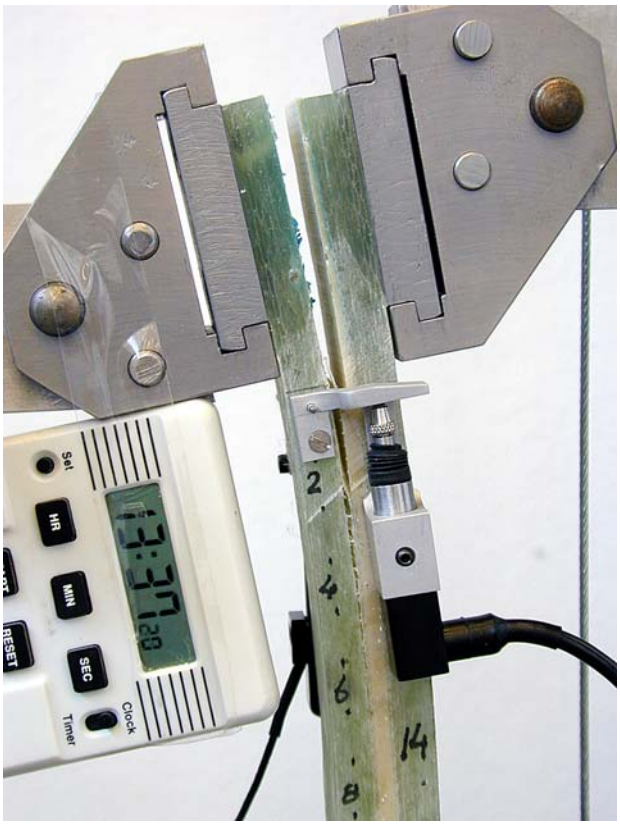

Figure 12. Photos of specimens subjected to different loading conditions, here expressed in terms of M_1/M_2. The measured phase angles of the end-opening are indicated in parenthesis. a) M_1/M_2 = -0.45 ($\varphi_0 \approx 26°$), b) M_1/M_2 = 0.48 (φ_0

≈ 53°), c) M_1/M_2 = 0.88 (φ_0 ≈ 68°). [Mix10_13_41_50.jpg; Mix08 027.jpg; Mix13_18.jpg]

4.2 Measured fracture resistance

J_R was calculated from equation (2), by the use of the following elastic data: E_1 = 4 GPa and E_2 = 34 GPa. Accounting for the adhesive layer is significant for the specimens evaluated here. Neglecting the adhesive layer, i.e. calculating J_R from the equation (1) (homogenous specimen), gave a value approximately 10 % lower than the sandwich equation (2).

Fig. 13 shows typical fracture resistance curves. With increasing phase angle the fracture resistance increases faster and reaches a higher steady-state level over smaller end-opening.

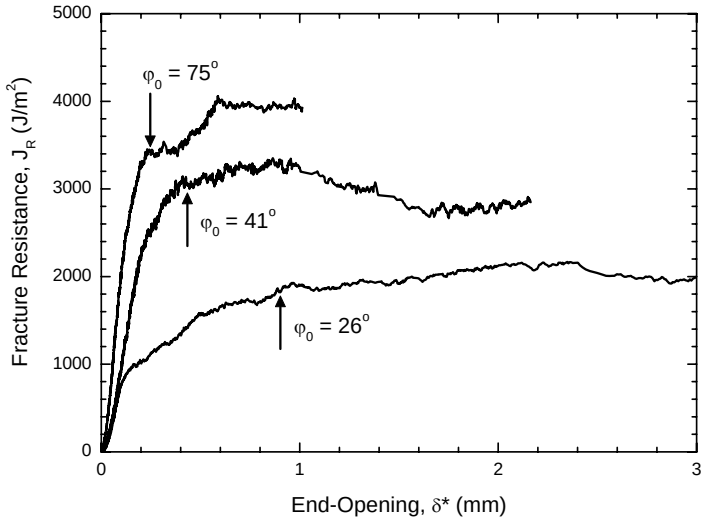

Figure 13. Measured fracture resistance, J_R, as a function of the end-opening for various values of the phase angle of the end-opening at the onset of steady-state. Onset of steady-state is indicated by arrows. [Mixed_10_11_14_1b.opj]

The steady-state fracture resistance, J_{ss}, is shown in Fig. 14 as a function of φ_0. For $0 < \varphi_0 < 50°$, J_{ss} is about 2.2 kJ/m^2. With increasing φ_0, J_{ss} increases to about 4.0 kJ/m^2.

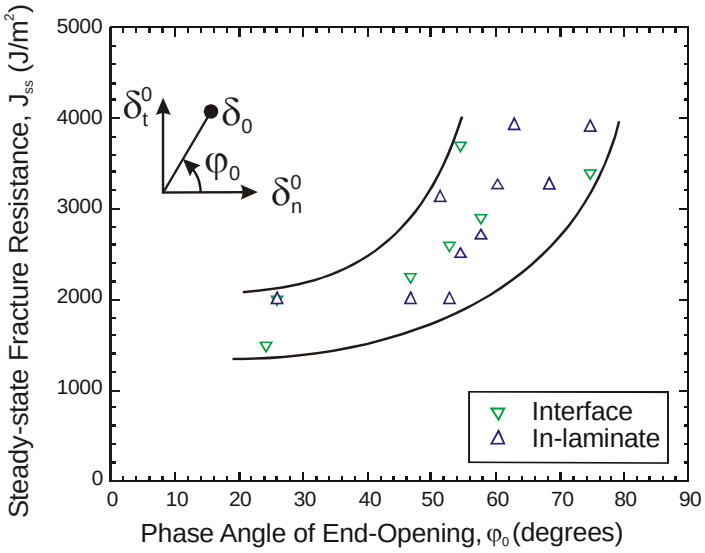

Figure 14. The measured steady-state fracture resistance as a function of the phase angle of opening, φ_0. Values for interfacial as well as delamination crack are shown. [Mixed_mode_results_overview_1d.opj]

The magnitude of the crack opening displacement at the point where the cohesive zone is fully developed is shown as a function of the phase angle in Fig. 15. Although the number of results is low for his preliminary study, a few observations can be made. Under dominating normal opening, δ_0 is on the order of one mm, broadly in agreement with earlier results under pure mode I (no tangential displacement) (Sørensen and Jacobsen, 1989; Feih et al., 2003). With increasing φ_0, the toughening is attained over a much smaller end opening.

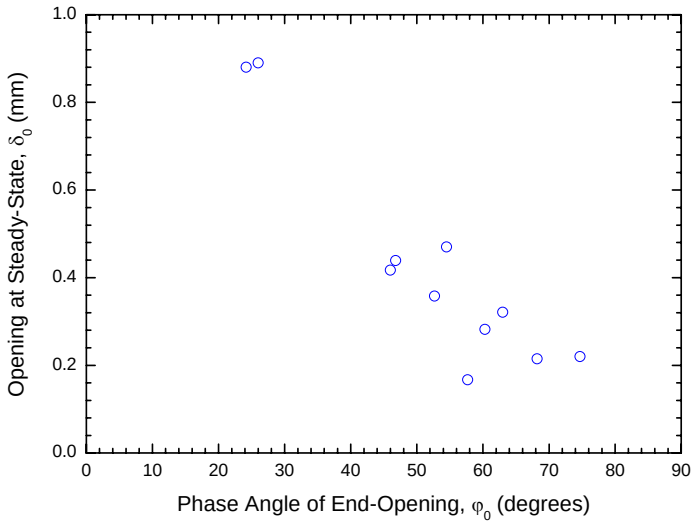

Figure 15. The magnitude δ_0 as a function of phase angle φ_0 of the end-opening of the fully developed cohesive zone. [Mixed_mode_results_overview_1e.opj]

Note that for all experiments $\delta_n^* > 0$ ($0° < \varphi_0 < 90°$) so that the crack faces are not expected to be in contact. Friction between the crack faces is thus minimal. The difference in the steady-state fracture resistance as a function of φ_0 can thus

be attributed to the nature of the crack bridging mechanism. Further studies at the microscale are necessary to clarify this point.

4.3 Determination of mixed mode cohesive laws

A third-order polynomial was fitted to the J_R-δ_n^*-δ_t^*-data; see Appendix B for details. The data used for fitting was the data ranging from the onset of crack growth to steady-state. The fitted function is shown in Fig. 16 for a rectangular domain given by $0 < \delta_n^* < 0.8$ mm and $0 < \delta_t^* < 0.4$ mm. This area is actually larger than the measured domain in which J_R increases from J_0 to J_{ss}, but this area is not rectangular. The rectangular area is chosen for illustrating purposes (data in a rectangular grid is easier to perceive than a domain having a non-regular shape).

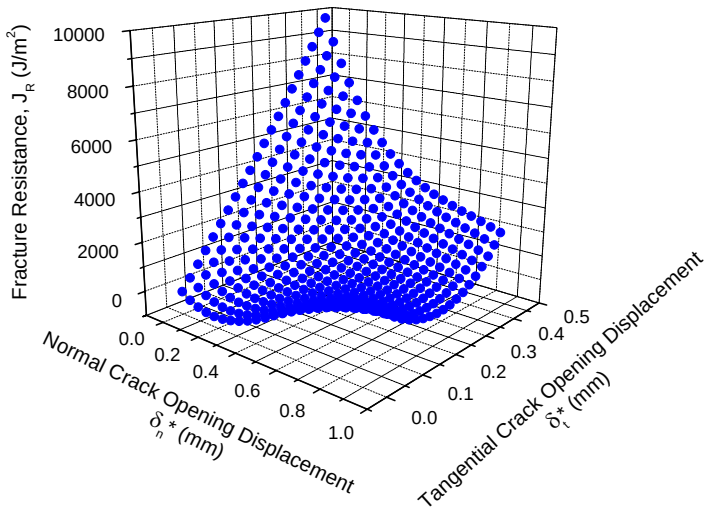

Figure 16. A three-dimensional plot showing the fitted J_R surface as a function of δ_n^* and δ_t^*. [Poly_fit_3D.opj]

In Fig. 17a) and b), the resulting cohesive stresses σ_{22} and σ_{12} are shown as functions of δ_n^* and δ_t^*. The most obvious observation is that σ_{12} is an order of magnitude larger than σ_{22}. Within the measured domain, where J_R rises, the absolute values about 20 MPa for σ_{12} and about 1 MPa for σ_{22}. Concerning σ_{12}, it is of interest that for small δ_n, σ_{12} is relative constant, i.e. independent of δ_n and δ_t. Unfortunately, due to the rather limited number of data sets having $0° < \varphi_0 < 45°$, the partial derivative $\partial J_R / \partial \delta_n^*$ (= σ_{22}) is subjected to larger uncertainties than $\partial J_R / \partial \delta_t^*$ (= σ_{12}) (some of the deducted σ_{22} values are actually negative, i.e. compressive, which is judged to be unrealistic). Therefore, no conclusions can be made regarding the shape of the σ_{22}-δ_n^*-δ_t^* surface. It should be noted, however, that independent measurements of cohesive laws due to fibre cross over bridging (Spearing and Evans, 1992; Sørensen and Jacobsen, 1998; Feih et

al., 2003) show that the cohesive stress under pure mode I cracking (i.e., $\delta_t = 0$) the cohesive stress σ_{22} starts at a few MPa's and decreases with increasing δ_n. Further studies at the macro and microscale are needed to shed more light on the crack bridging mechanisms.

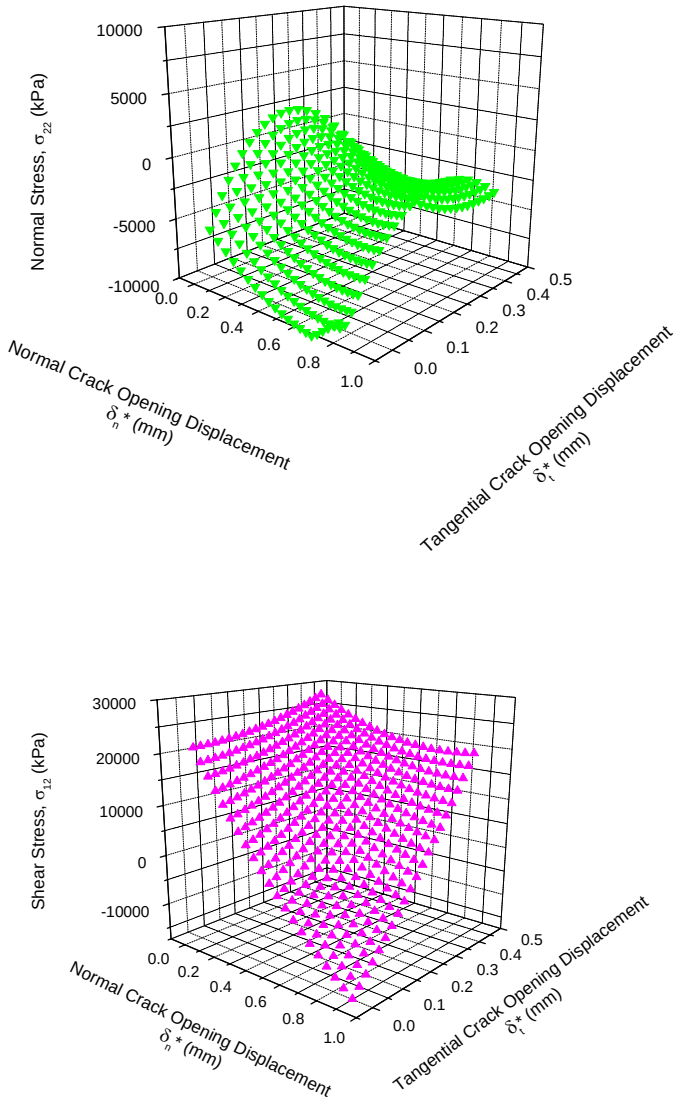

Figure 17. Three-dimensional plots showing (a) σ_{22} and (b) σ_{12} as a function of δ_n^* and δ_t^*. [Poly2fit_3D.opj]

5 Discussion

5.1 Advantages and drawbacks of the experimental approach

The primary advantage of the present approach is that mixed mode cohesive law can be determined directly from measured data. No finite element simulations of the specimens are required.

An obvious drawback is that the present approach requires a special fixture, but so do other mixed mode specimens (Reeder and Crews, 1992; Shivakumar et al., 1998). The popular mixed mode bending methods of Reeder and Crews (1992) only provides stable crack growth under dominating mode I cracking; under dominating mode II, the crack growth can be unstable (Kim and Mayer, 2003).An advantage of the present method is that crack growth is stable over the entire mode mixity from pure mode I to pure mode II. Then, fracture energy can be determined from arrested cracks having truly sharp tips. The measurement is therefore not sensitive to details of the crack starter (notch or film insert). Furthermore, to obtain as much as possible of the early part of the cohesive laws, a procedure involving pre-cracking and renotching (machining) and reloading are necessary. This is somewhat time consuming. The test itself however is fast to perform.

5.2 On the use of a displacement potential for cohesive laws

The assumption that a displacement potential (equation (9)) exists requires that the toughness increase is history-independent and depends only upon the present end-opening and end-sliding, δ_n^* and δ_t^*. A critical test is therefore to reach the *same* values of δ_n^* and δ_t^* through *differen*t monotonic loading-histories. If the toughness increase follows the displacement potential, the same J_R will be attained at the same δ_n^* and δ_t^* values, irrespective of the different load-paths. However, for the test method presented here, the ratio M_1/M_2 remains fixed during a load-unload sequence. It is thus not possible with this specimen to check experimentally whether the toughness increase is actually history-independent or not. Further ideas must be developed to verify whether or not this assumption is full filled. This is however, outside the scope of the present paper.

When a displacement potential is used, the fracture toughness increase is given by the end-opening of the cohesive zone. This has interesting consequences from the point of view of modelling. Assume that the mixed mode cohesive law has been determined correctly and is to be used in a model for strength prediction of a component. What matters is thus that the model provides correct δ_n^* and δ_t^* values. In finite element models, the displacements are the primary output (stresses and strain are determined less accurately since they are derived from the displacement field). Thus, it can be expected that modelling of any specimen the use of a relative coarse mesh still give accurate tough-

ening predictions. The approach is thus expected to be well suited for modelling of failure evolution in large structures. These comments are only valid, of course, if the material outside the failure process zone obeys elasticity, as it has been presumed throughout the entire paper.

6 Summary and conclusions

A mixed mode test specimen, the DCB specimen loaded with uneven bending moments at the two beams, was proposed for fracture mechanics characterisation of mixed mode cracking. A special loading fixture based on steel wires was developed.

Crack propagation in adhesive joints between glass-fibre laminates was investigated for various mode mixity conditions. In the early stages of cracking, the crack propagated along the adhesive/laminate interface; fibre cross over bridging occurred. After some crack extension, a new crack formed at the next interface within the laminate; fibre bridging also occurred here. The fibre bridging resulted in rising crack growth resistance. Cohesive laws (relationship between crack opening and sliding and the normal and shear stress transmitted by the bridging ligaments) were determined by a J integral approach. The deducted normal stress was found to be low, in the order of 1 MPa (broadly consistent with earlier mode I results) whereas the shear stress was found to be about 20 MPa. The shear stress value was relative insensitive to the actual value of the normal and tangential crack opening displacements. Effects of opening and tangential crack opening displacements on the normal stress could not be determined, due to the low number of specimen tested under dominating normal crack opening displacement.

Acknowledgements

This work was supported by the Danish Ministry of Environment and Energy through an EFP2001-fund 1363/01-007. Thanks to Jens Olsson, Claus Mikkelsen and Erik Vogeley for experimental help and Bjørn S. Johansen and Peter Kirkegaard for help with the numerical differentiation.

References

Albertsen, H., Ivens, J., Peters, P. Wevers, M., and Verpost, I, 1995, "Interlaminar fracture toughness of CFRP influenced by fibre surface treatment: part 1. Experimental results", Composite Science and Technology, vol. 54, 133-45.

Bao, G. and Suo, Z., 1992, "Remarks on crack-bridging concepts", Applied Mech. Rev., vol. 45, pp. 355-61.

Cao, H. C., and Evans, A. G., 1989, "An experimental study of the fracture resistance of bimaterial interfaces", Mechanics of Materials, Vol. 7, pp. 295-304.

Cox, B. N., and Marshall, D. B., 1991, "The determination of crack bridging forces", Int. J. Fracture, Vol. 49, pp. 159-76.

Dundurs, J., 1969, "Discussion on 'Edge-bonded dissimilar orthogonal elastic wedges under normal and shear loading'", J. Appl. Mech., Vol. 36, pp. 650-2.

Evans, A. G., and Hutchinson, J. W., 1989, "Effect of non-planarity on the mixed mode fracture resistance of bimaterial interfaces", Acta Metall., Vol. 37, pp. 909-16.

Feih, S. Wei, J. Kingshott, P. and Sørensen, B. F., 2003, "The influence of fibre sizing on the strength and fracture toughness of glass fibre composites", Composites part A. submitted.

Foote, R. M. L., Mai, Y.-W., and Cotterell, B., 1986, "Crack growth resistance curves in strain-softening materials", J. Mech. Phys. Solids, Vol. 34, pp. 593-607.

Freiman, S. W., Mulville, D. R., and Mast, P. W., 1973, "Crack propagation studies in brittle materials", Journal of Materials Science, Vol. 8, pp. 1527-33.

Hashemi, S., Kinloch, A. J., and Williams, J. G., 1990, "The analysis of interlaminar fracture in unidirectional fibre-polymer composites", Proc. R. Soc. Lond., Vol. A 427, pp. 173-90.

Hutchinson, J. W., and Suo, Z., 1992, "Mixed mode cracking in layered materials", in Advanced in Applied Mechanics, Vol. 29 (Ed. J. W. Hutchinson and T. Y. Wu), Academic Press, Inc., Boston, pp. 63-191.

Jensen, H. M., Hutchinson, J. W., and Kim, K.-S., 1990, Decohesion of a cut prestressed film on a substrate", Int. J. Solid Structures, Vol. 26, pp. 1099-1114.

Kafkalidis, M. S. and Thouless, M. D., 2002, "The effect of geometry and material properties of the fracture of single lap-shear joints", Int. J. Solids Structures, Vol. 39, pp. 4367-83.

Kim, B. W, and Mayer, A. H., 2003, "Influence of fiber direction and mixed-mode ration on the delamination fracture toughness of carbon/epoxy laminates", Composite Science and Technology, Vol. 63, pp. 695-713.

Kinlock, A. J., 1987, Adhesion and Adhesives, Science and Technology, Chapman and Hall, London.

Liang, Y. -M., and Liechti, K. M., 1995, "Toughening mechanisms in mixed mode interfacial fracture", Int. J. Solids Structures, Vol. 32, pp. 957-78.

Liechti, K. M., and Chai, Y. -S., 1992, "Asymmetric shielding in interfacial fracture under in-plane shear", Journal of Applied Mechanics, Vol. 59, pp. 295-304.

Liechti, K. M., and Wu., J.-D., 2001, "Mixed mode, time-dependent rubber/metal debonding", Mech. Phys. Solids, Vol. 49, pp. 1039-72.

Matthews, F. L.,1987, Joining Fibre-Reinforced Plastics, Elsevier Applied Science, London.

Mohammad, I., and Liechti, K. M., 2000, “Cohesive zone modelling of crack nucleation at bimaterial corner”, J. Mech. Phys. Solids, Vol. 48, pp. 735-64.

Ozdis, F., and Carlsson, L. A., 2000, "Characterisation of mixed mode delamination growth in glass/epoxy composite cylinders", J. Comp. Mater., Vol. 33, pp. 420-41.

Reeder, J. R., and Crews Jr, J. H., 1992, "Redesign of the mixed-mode bending delamination testing", J. Composite Technology Research, Vol. 14, pp. 12-19.

Rice, J. R., 1968, "A path independent integral and the approximate analysis of strain concentrations by notches and cracks", J. Appl. Mech., Vol. 35, pp. 379-86.

Rice, J. R., 1988, "Elastic fracture mechanics concepts for interfacial cracks", J. Appl. Mech., Vol. 55, pp. 98-103.

Shivakumar, K. N., Crews, J. R. Jr., Avva, V. S., 1998, "Modified mixed-mode bending test apparatus for measuring delamination fracture toughness of laminated composites", J. Comp. Mater., Vol. 32, pp. 804-28.

Suo, Z., 1990, "Delamination specimens for orthotropic materials", Journal of Applied Mechanics, Vol. 57, pp. 627-34.

Suo, Z., and Hutchinson, J. W., 1989, "On sandwich test specimen for measuring interface crack toughness", Mater. Sci. Engng. Vol. A 107, pp. 135-42.

Suo, Z., and Hutchinson, J. W., 1990, "Interface crack between two elastic layers", *Int. J. Fract.*, Vol. 43, pp. 1-18.

Suo, Z., Bao, G., and Fan, B., 1992, "Delamination R-curve phenomena due to damage", J. Mech. Phys. Solids., Vol. 40, pp. 1-16.

Sørensen, B. F. and Jacobsen, T. K., 1998, "Large scale bridging in composites: R-curve and bridging laws", Composites part A, vol. 29A, pp. 1443-51.

Sørensen, B. F. and Jacobsen, T. K., 2000, "Crack growth in composites: Applicability of R-curves and bridging laws", Plastic Rubber and Composites, Processing and Application, Vol. 29, pp. 119-33.

Sørensen, B. F., Brethe, P. and Skov-Hansen, P., 1996, "Controlled Crack Growth in Ceramics: The DCB-Specimen Loaded with Pure Moments", J. Euro. Ceram. Soc., Vol. 16, pp. 1021-5.

Thouless, M. D., and Evans, A. G., 1990, "Comment on the spalling and edge - cracking of plates", Scripta Metall. Mater., Vol. 24, pp. 1507-10.

Thouless, M.D., 1990, "Fracture of a model interface under mixed mode loading", Acta Metall., Vol. 38, pp. 1135-40.

Tvergaard, V., and Hutchinson, J. W., 1993, "The influence of plasticity on mixed mode interface toughness", Journal of the Mechanics and Physics of Solids, Vol. 41, pp. 1119-35.

Wang, J. S. and Suo, Z., 1990, "Experimental determination of interfacial toughness curves using brazil-nut-sandwiches", Acta Metall. Mater., Vol. 38, pp. 1279-90.

Williams, J. G., 1989, "Fracture mechanics of anisotropic materials", in Application of Fracture Mechanics to Composite Materials (Ed. K. Friederich), Elsevier Science Publishers.

Yang, Q. D., Thouless, M. D., and Ward, S. M., 1999, "Mixed-mode fracture analyses of plastically-deforming adhesive joints", Int. J. Fracture, Vol. 110, pp. 175-87.

Östlund, S., 1995, "Fracture modelling of brittle-matrix composites with spatially dependent crack bridging", Fatigue Frac. Engng. Mater. Struct., Vol. 18, pp. 1213-30.

Østergaard, R. C., and Sørensen, B. F., 2003, "Interface crack in isotropic sandwich structures", Int. J. Fracture. In preparation.

List of symbols

d	distance between measurements points
h	thickness of core layer in sandwich specimens
ℓ	moment arm
s	spacing between the rollers
B	width of specimen
D	position of the neutral axis of a bimaterial beam
E	Young's modulus
E_1	Young's modulus of core material in sandwich specimens
E_2	Young's modulus of beam material in sandwich specimens
H	beam height
I_0	non-dimensional parameter
I_1	non-dimensional parameter
J_0	initial value of fracture resistance
J_{ext}	J integral evaluated along external boundaries
J_{loc}	J integral evaluated just outside the failure process zone
J_R	fracture resistance
J_{ss}	steady-state value of the fracture resistance
J_{tip}	J integral evaluated just around the crack tip
K	complex stress intensity factor of interface crack ($K = K_1 + iK_2$)
K_I	mode I stress intensity factor
K_{II}	mode II stress intensity factor
M_1	moment applied to beam # 1
M_2	moment applied to beam # 2
P	applied force
R	radius of roller
ε	bimaterial constant
δ	magnitude of crack opening
δ_0	magnitude of opening at which the cohesive stresses vanish
δ_n	normal component of crack opening displacement
δ_n^*	normal component of end-opening
δ_t	tangential component of crack opening displacement
δ_t^*	tangential component of end-opening
δ_m	measured crack opening displacement
ψ	phase angle of stress intensity factor
$\hat{\psi}$	phase angle of complex interface stress intensity factor
ν	Poisson´s ratio
η	ratio between thickness of core and beam ($\eta = h/H$)
φ	phase angle of the crack opening
φ_0	phase angle of the opening at which the cohesive stresses vanish
σ_{22}	normal stress component, acting normal to the crack plane
σ_{12}	shear stress component at the crack plane
Δ	non-dimensional measure of position of neutral axis ($\Delta = D/h$)

Γ_{ext} integration path along the external boundaries of a specimen
Γ_{loc} integration path along the failure process zone
Φ displacement potential function

Appendix A: Non-dimensional parameters for the analysis of sandwich specimen

The geometry of the sandwich specimen is shown in Fig. 2. Here, H is the thickness of the skin layers (made of material #1), h is the thickness of the core layer (made of material #2), and D denotes the position (measured from the top of the skin layer) of the neutral axis of the bimaterial beam. The non-dimensional parameters η, I_0 and I_1 used in equation (2) are defined as follows (Østergaard and Sørensen, 2003):

$$I_0 = \frac{1}{3}\frac{1}{\eta^3} - \frac{\Delta}{\eta^2} + \frac{\Delta^2}{\eta} + \Sigma\left(\frac{1}{\eta^2} + \frac{1}{\eta} + \Delta^2 - 2\frac{\Delta}{\eta} - \Delta + \frac{1}{3}\right), \tag{A-1}$$

$$\eta = \frac{h}{H}\ , \tag{A-2}$$

and

$$I_1 = \frac{1}{12}\left(\Sigma + \frac{8}{\eta^3} + \frac{12}{\eta^2} + \frac{6}{\eta}\right)\ . \tag{A-3}$$

The stiffness ratio parameter, Σ, is defined as (plane strain)

$$\Sigma = \frac{E_1}{E_2}\frac{1-\nu_2^2}{1-\nu_1^2}\ , \tag{A-4}$$

where E_1 and E_2 are the Young's' moduli of material #1 and #2, respectively. For plane stress (A-4) becomes $\Sigma = E_1/E_2$. The parameter Δ is a non-dimensional measure of the position of the neutral axis

$$\Delta = \frac{D}{h} = \frac{1 + 2\Sigma\eta + \Sigma\eta^2}{2\eta(1+\Sigma\eta)}\ . \tag{A-5}$$

The parameters I_0, η, Σ and Δ are identical to the ones derived by Suo and Hutchinson (1990) in their analysis of bimaterial fracture specimens.

Appendix B: Effects of finite displacement, rotation and friction

As the specimen is loaded and begins to crack, the ends of the DCB-beams deflect and rotate. The transverse beams also move and rotate, since they are fixed to the ends of the DCB-specimen. Both the displacement and rotation cause the true moments to differ from the nominal moments, equation (16). The moments are created by a wire that runs through rollers arranged as shown in Fig.B-1. Thus, the true moment arm is

$$\ell = 2R + s\cos\theta, \qquad \text{(B-1)}$$

where R is the radius of the rollers and s is the spacing between the centres of the rollers, measured along the transverse beam arm. In order to reduce the effect of rotation, the transverse arms were angled 10 degrees in the direction opposite of the rotation that they would undergo during loading. Thus, the transverse beam (the moment arm) reaches the neutral position ($\theta = 0°$) after a rotation of 10 degrees. With this design, the error in the applied moment will always be less than 6% as long as the beam-ends rotate less than 20 degrees. Note from (B-1) that decreasing the spacing between the rollers s, decreases the error. Thus, in most cases, the error will be significantly smaller than 6%.

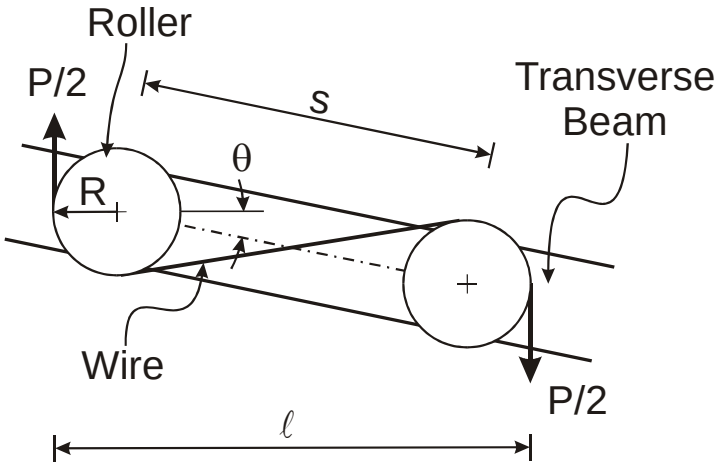

Figure B-1. Geometric relationship between transverse beam rotation angle θ and moment arm ℓ. [Beam_arm_rotation_1a.cdr]

In order to minimize the effect of the transverse displacement of the transverse beams, the vertical distance (the x_1-direction, Fig. 7) between rollers at the upper and lower parts of the test machine should be maximized. In our set-up, this distance exceeds 2 m, so the error in the moment is vanishing.

The friction in the rollers (mounted at ball bearings) and wires were measured by pulling the wire along its direction. The friction was found to increase linearly with the applied load. Based on these experiments, the frictional moment

during testing was estimated to be less than 3% of the applied moment, i.e. so small that it could be neglected.

Appendix C: Approach for determining cohesive laws

A polynomial of the form $z = f(x, y)$ was fitted to the J_R- δ_n^* - δ_t^* -data, with z representing J_R, x being δ_n^* and y being δ_t^*. A third order polynomial was found to give the best fit (since, in this preliminary study, the number of test is lower than the number that normally would be conducted, a higher order polynomial might be feasible for other tests). The function f was then given by

$$f(x, y) = A_0 + A_1x + A_2y + A_3x^2 + A_4y^2 + A_5xy + A_7x^3 + A_8x^2y + A_9xy^2 + A_{10}y^3$$

where the A's are fitting constants determined so that they provide the least squares fit to the data points. The coefficients were found by the solution of the normal equations for the problem. Having determined the A's, it is straightforward to determine the partial derivatives, $\partial f/\partial x$, and $\partial f/\partial y$, that, according to (12), represents σ_{22} and σ_{12}, respectively.

Bibliographic Data Sheet **Risø-R-1394(EN)**

Title and authors

A general mixed mode fracture mechanics test specimen: The DCB-specimen loaded with uneven bending moments

Bent F. Sørensen[a], Kenneth Jørgensen[a], Torben K. Jacobsen[b], and Rasmus C. Østergaard[a]

[a]Materials Research Department, Risø National Laboratory, 4000 Roskilde, Denmark

[b]LM Glasfiber, Rolles Møllevej 1, DK-6640 Lunderskov, Denmark

ISBN	ISSN
87-550-3186-2 87-550-3187-0(Internet)	0106-2840

Department or group	Date
Materials Research Department	15 March 2004

Groups own reg. number(s)	Project/contract No(s)
	ENS-1363/01-0007

Sponsorship

Danish Energy Authority, the Ministry of Economics and Business Affairs

Pages	Tables	Illustrations	References
35	0	18	39

Abstract (max. 2000 characters)

A mixed mode specimen is proposed for fracture mechanics characterisation of adhesive joints, laminates and multilayers. The specimen is a double cantilever beam specimen loaded with uneven bending moments at the two free beams. By varying the ratio between the two applied moments, the full mode mixity range from pure mode I to pure mode II can be generated for the same specimen geometry. The specimen allows stable crack growth. In case of large scale crack bridging, mixed mode cohesive laws can be obtained by a J integral based approach. As an example, fracture of adhesive joints between two glass-fibre laminates was studied. The mixed mode fracture resistance increased with increasing crack length due to fibre bridging, eventually reaching a steady-state level (R-curve behaviour). The steady-state fracture toughness level increased with increasing tangential crack opening displacement.

Descriptors INIS/EDB

ADHESION; BENDING; COMPOSITE MATERIALS; FACTRURE MECHANICS; FIBERGLASS; JOINTS; MATERIALS TESTING; SHEAR; STRESSES